



HAL
open science

Dynamics of Nanosecond Laser Pulse Propagation and of Associated Instabilities in a Magnetized Underdense Plasma

Weipeng Yao, A. Higginson, J.-R Marquès, P. Antici, J. Béard, K. Burdonov, M. Borghesi, A. Castan, A. Ciardi, B. Coleman, et al.

► **To cite this version:**

Weipeng Yao, A. Higginson, J.-R Marquès, P. Antici, J. Béard, et al.. Dynamics of Nanosecond Laser Pulse Propagation and of Associated Instabilities in a Magnetized Underdense Plasma. *Physical Review Letters*, 2023, 130 (26), pp.265101. 10.1103/PhysRevLett.130.265101 . hal-04161009

HAL Id: hal-04161009

<https://hal.sorbonne-universite.fr/hal-04161009>

Submitted on 24 Jul 2023

HAL is a multi-disciplinary open access archive for the deposit and dissemination of scientific research documents, whether they are published or not. The documents may come from teaching and research institutions in France or abroad, or from public or private research centers.

L'archive ouverte pluridisciplinaire **HAL**, est destinée au dépôt et à la diffusion de documents scientifiques de niveau recherche, publiés ou non, émanant des établissements d'enseignement et de recherche français ou étrangers, des laboratoires publics ou privés.

Dynamics of nanosecond laser pulse propagation and of associated instabilities in a magnetized underdense plasma

W. Yao,^{1,2,*} A. Higginson,³ J.-R. Marquès,¹ P. Antici,⁴ J. Béard,⁵ K. Burdonov,^{1,2,6} M. Borghesi,⁷ A. Castan,^{1,8} A. Ciardi,² B. Coleman,⁷ S. N. Chen,⁹ E. d’Humières,¹⁰ T. Gangolf,¹ L. Gremillet,^{8,11} B. Khair,¹² L. Lancia,¹ P. Loiseau,^{8,11} X. Ribeyre,¹⁰ A. Soloviev,¹³ M. Starodubtsev,¹³ Q. Wang,^{14,15} and J. Fuchs^{1,†}

¹*LULI - CNRS, CEA, UPMC Univ Paris 06 : Sorbonne Université,
Ecole Polytechnique, Institut Polytechnique de Paris - F-91128 Palaiseau cedex, France*

²*Sorbonne Université, Observatoire de Paris, Université PSL, CNRS, LERMA, F-75005, Paris, France*

³*Center for Energy Research, University of California San Diego,
9500 Gilman Drive, La Jolla, California 92093-0417, USA*

⁴*INRS-EMT, 1650 boul. Lionel-Boulet, Varennes, QC, J3X 1S2, Canada*

⁵*CNRS, LNCMI, Univ Toulouse 3, INSA Toulouse,
Univ Grenoble Alpes, EMFL, 31400 Toulouse, France*

⁶*JIHT, Russian Academy of Sciences, 125412, Moscow, Russia*

⁷*School of Mathematics and Physics, The Queen’s University Belfast, Belfast, UK*

⁸*CEA, DAM, DIF, F-91297 Arpajon, France*

⁹*“Horia Hulubei” National Institute for Physics and Nuclear Engineering, RO-077125 Bucharest-Magurele, Romania*

¹⁰*University of Bordeaux, CELIA, CNRS, CEA, UMR 5107, F-33405 Talence, France*

¹¹*Université Paris-Saclay, CEA, LMCE, 91680 Bruyères-le-Châtel, France*

¹²*Office National d’Etudes et de Recherches Aérospatiales (ONERA), Palaiseau 91123, France*

¹³*IAP-RAS, Nizhny Novgorod, Russia*

¹⁴*Institute of Applied Physics and Computational Mathematics, Beijing 100094, China*

¹⁵*Department of Electrical and Computer Engineering, University of Alberta,
9211 116 St. NW, Edmonton, Alberta T6G 1H9, Canada*

(Dated: May 30, 2023)

The propagation and energy coupling of intense laser beams in plasmas are critical issues in inertial confinement fusion. Applying magnetic fields to such a setup has been shown to enhance fuel confinement and heating. Here we report on experimental measurements demonstrating improved transmission and increased smoothing of a high-power laser beam propagating in a magnetized underdense plasma. We also measure enhanced backscattering, which our kinetic simulations show is due to magnetic confinement of hot electrons, thus leading to reduced target preheating.

The propagation and energy coupling of intense laser pulses in underdense plasmas, defined as having electron density $n_e < n_c \equiv 10^{21} \lambda_{\mu\text{m}}^{-2} \text{ cm}^{-3}$ (n_c is the critical plasma density at which the electron plasma frequency equals the frequency of the incident laser wave, of wavelength $\lambda_{\mu\text{m}}$ in μm) have been extensively researched, because of their paramount importance to laser-driven inertial confinement fusion (ICF) [1–3]. For ICF, it is critical that as much as possible of the laser energy be transferred either directly to the fuel in direct drive [4], or to the hohlraum walls in indirect drive [5], and this in a spatially uniform manner, as the laser’s imprint seeds hydrodynamic instabilities that limit fuel compression [6]. Laser-plasma interaction (LPI) can be either beneficial to ICF, e.g. when spatially smoothing the laser energy distribution [7, 8], or detrimental, e.g. by conversely causing strong inhomogeneities in the laser pattern through self-focusing [9, 10], or by inducing energy loss through stimulated Raman and Brillouin scattering (SRS and SBS, respectively) [11]. The former scattering mechanism can further induce, through the generation of forward-propagating hot electrons, detrimental preheating of the fuel, setting an upper limit on the laser intensity used in ICF [12].

In the quest for better performance of ICF, applying external magnetic (B) fields to indirect-drive targets [13, 14] has been shown [15] to improve the fuel heating and could help mitigating hydrodynamic instabilities [16]. Yet magnetization effects can impact the laser propagation [17] and LPI processes [18] in a nontrivial manner, notably in the context of magnetized liner inertial fusion (MagLIF) [19, 20]. Prior works have investigated, both theoretically [21, 22] and experimentally [14], how a B field parallel to the laser path alters the laser propagation and instabilities. However, when the B field is not simply parallel to the laser, there is yet no clear understanding [23–25], nor detailed experimental investigation, of its effects.

In this paper, we experimentally explore the dynamics of a single laser beam propagating through an underdense magnetized plasma [26–28]. The low-density plasma explored here (from 0.02 to 0.08 n_c) is used as a proxy for the gas fill of indirect-drive ICF hohlraums (spanning 0.01 – 0.1 n_c , for a 351 nm laser wavelength [29]). In our setup, a large-scale ($\sim \text{cm}$), strong ($\sim 20 \text{ T}$) magnetic field can be applied to the target, perpendicularly to the laser path. Note that this setup is not geared to be compact as the one deployed around hohlraums

[15], but it offers the advantage of being non-destructive, steady-state ($> 100 \mu\text{s}$) and homogeneous ($\sim 1 \text{ cm}$) relative to the plasma dynamics and scale. Compared to the unmagnetized case, we report, via time-resolved and two-dimensional (2D) transverse imaging of the transmitted beam, on enhanced energy transmission and beam smoothing in a magnetized plasma. These results are ascribed to the increased plasma heating due to inhibited electron thermal transport across the B field [30], as indicated by large-scale, three-dimensional (3D) magnetohydrodynamic (MHD) simulations. Furthermore, while the level of backscattered SRS remains very weak ($\sim 10^{-5}$ of the laser energy), it appears to be enhanced in the magnetized case. 2D particle-in-cell (PIC) simulations confirm this trend and reveal that it results from the magnetic confinement of the SRS-generated hot electrons, a possibly beneficial effect in terms of fuel preheating.

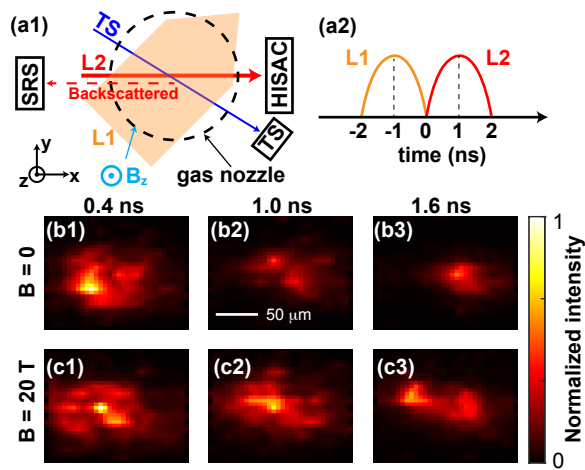


FIG. 1. (a1) Sketch of the experimental setup (top view, see text for details). (a2) Time sequence of the preheating (L1) and interaction (L2) laser beams. (b-c) Temporal snapshots from the HISAC diagnostic, displaying the transmitted L2 light for a peak electron density $n_e = 0.04n_c$ and a magnetic field (b) $B = 0$ and (c) $B = 20 \text{ T}$. For visualization purposes, all panels are normalized to their respective maximum intensity (i.e. the brightest pixel in each image is set to 1) and share the same colormap.

The experiment was performed at the Laboratoire pour l'Utilisation des Lasers Intenses LULI2000 facility. As shown in Fig. 1(a), it made use of two laser beams, both having a $1.053 \mu\text{m}$ wavelength and a Gaussian temporal profile with 1 ns full-width-at-half-maximum (FWHM) duration. The first one (L1), of $\sim 30 \text{ J}$ energy, served to preionize a hydrogen gas jet, delivered by a supersonic gas nozzle of 2 mm-diameter aperture. It was focused to a large spot of $2 \times 0.3 \text{ mm}^2$ (horizontal and vertical FWHM sizes, respectively), resulting in an on-target intensity of $3 \times 10^{12} \text{ W cm}^{-2}$. The main interaction beam (L2), propagating along the x -axis and polarized along the z -axis, was shot at the center of the

fully ionized hydrogen plasma, during the falling edge of L1 [see Fig. 1(a2)]. It was focused using an $f/22$ lens into a single speckle of $70 \times 70 \mu\text{m}^2$ (FWHM) size and $\sim 2 \text{ mm}$ Rayleigh length. It contained a $\sim 50 \text{ J}$ energy, yielding an intensity at focus of $I_0 \sim 1.4 \times 10^{15} \text{ W cm}^{-2}$. Both laser beams propagated at 0.75 mm above the nozzle opening. The plasma profile had a length of 1.5 mm (FWHM), and its peak electron density was varied in the range $n_e = 0.02 - 0.08 n_c$ by adjusting the backing pressure of the gas jet system. The underdense plasma mimics the hohlraum environment where LPI processes mainly arise in indirect-drive ICF. The external $\sim 20 \text{ T}$ B field, generated by a pulsed-power driven Helmholtz coil [31, 32], was directed along the gas flow axis (i.e. the positive z -axis).

The transmitted L2 beam was characterized by collecting the on-axis light exiting the plasma using a lens of aperture ($f/10$) larger than that of the focusing lens ($f/22$). The laser's focal spot was imaged onto a high-speed, 2D spatially-resolved sampling camera (HISAC) composed of a fiber optics bundle coupled to a streak camera of 30 ps temporal resolution [33, 34]. Additionally, the electron plasma waves were interrogated via Thomson scattering (TS) of a probe beam of $0.527 \mu\text{m}$ wavelength, $\sim 1 \text{ ns}$ FWHM duration, and $\sim 300 \mu\text{m}$ focal spot [30], allowing the electron number density (n_e) and temperature (T_e) to be measured at the center of the focal spot of L2. Finally, both time-resolved and time-integrated measurements were made of the backscattered laser light due to SRS and SRS, collected within the full aperture of the L2 focusing optics, as commonly performed in ICF experiments to assess LPI processes [35].

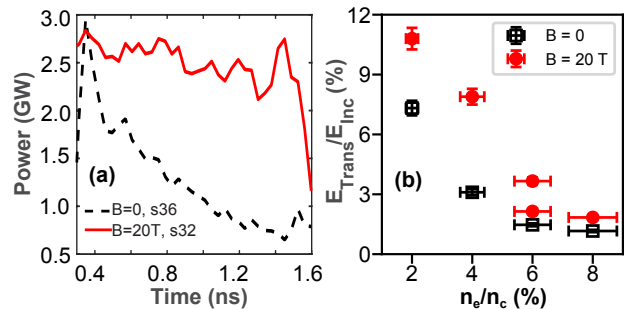


FIG. 2. (a) Time-resolved transmitted power through the gas plasma of peak electron density $n_e = 0.04n_c$, magnetized (red solid curve) or not (black dashed curve), as measured by the HISAC diagnostic. (b) Time-integrated transmitted energy (normalized to the incident laser energy), measured with HISAC as a function of the peak plasma electron density, with (red) or without (black) the external B field. The electron density is that of the fully ionized gas jet, based on off-line calibration with the neutral gas. The horizontal error bars represent the calibration uncertainty, while the vertical error bars represent the noise level of the corresponding shots.

We first discuss the increased laser transmission and smoothing achieved in the magnetized case. Figures 1(b)

and (c), as well as Fig. 2 summarize the HISAC measurements. The reconstructed HISAC snapshots are shown in Figs. 1(b) and (c), from 0.4 ns to 1.6 ns after the start of L2, for a peak density of $n_e = 0.04n_c$. In the unmagnetized case, the transmitted light signal is clearly decreasing with time, both in strength [Fig. 2(a)] and size [Fig. 1(b)]. The low absolute level of transmission, i.e., within 10% of the energy of the incident laser, is partially due to the laser's self-focusing and filamentation through the plasma [9, 10, 12], causing most of the transmitted beam energy to miss the HISAC collecting aperture. Strong ponderomotive self-focusing is expected under our experimental conditions. The associated intensity threshold [11] is indeed around $4 \times 10^{12} \text{ W cm}^{-2}$, i.e., well below the L2 intensity. Moreover, the self-focusing growth rate in the unmagnetized regime is $\Gamma_{sf} \simeq 0.125 (v_{osc}/v_{te})^2 \omega_{pe}^2/\omega_0$ [11] (ω_0 is the laser frequency, ω_{pe} the electron plasma frequency, v_{te} the electron thermal velocity and v_{osc} the electron oscillation velocity in the laser field), yielding a growth time $\Gamma_{sf}^{-1} \simeq 0.3 \text{ ps}$ for $T_e = 100 \text{ eV}$ (as inferred from TS), much smaller than the laser duration. In a magnetized plasma, however, as indicated by previous measurements [30] and our numerical simulations (see below), the electron density is lower and the electron temperature is higher. Since $\Gamma_{sf} \propto \omega_{pe}^2/v_{te}^2 \propto n_e/T_e$, one expects self-focusing to be weaker than in the unmagnetized plasma.

This prediction coincides with our observation that, in the magnetized regime, the transmitted light keeps both its strength [Fig. 2(a)] and transverse extent [Fig. 1(c)]. Figure 2(a) shows the transmitted light power as a function of time for a peak electron density of $n_e = 0.04n_c$. More energy is found to be transmitted when $B = 20 \text{ T}$, particularly at later times. The fraction of transmitted to incident light energy is plotted in Fig. 2(b) as a function of the peak electron density. The applied B field is seen to enhance the laser transmission over the full density range investigated, yet the effect is more pronounced at densities $n_e \lesssim 0.04n_c$.

The increased laser transmission through the magnetized plasma is favored not only by mitigated ponderomotive self-focusing, as mentioned above, but also by reduced absorption in the more dilute and hotter plasma [30]. These two trends are consistent with the expected inhibition of the electron thermal transport across the B field when the electron Hall parameter fulfills $H_e = \omega_{ce}\tau_{ei} > 1$ (ω_{ce} is the electron cyclotron frequency and τ_{ei} the electron-ion collision time). Using the values $n_e \simeq 0.02n_c$ and $T_e \simeq 100 \text{ eV}$ as estimated from the TS diagnostic and supported by 3D MHD simulations (Fig. 3), we obtain $H_e \approx 10$, thus indicating strong electron confinement perpendicular to the B field. Under such plasma conditions, the L2 laser experiences a lower inverse Bremsstrahlung absorption rate [36], which is another possible explanation for the increased laser transmission observed in Fig. 2(b). Note that the ther-

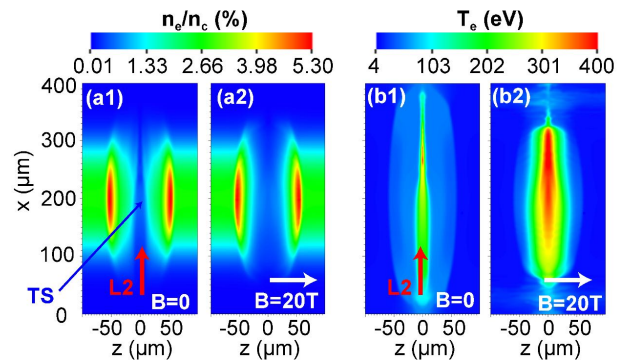


FIG. 3. 3D MHD simulation of the L1 and L2 beam-plasma interaction: 2D (xz) slices at $y = 0$ of the (a) electron number density and (b) temperature, in the (a1,b1) unmagnetized and (a2,b2) magnetized case. The initial peak electron density is $n_e = 0.04n_c$. All results are recorded at time $t = 1 \text{ ns}$ and displayed in logarithmic scale.

mal plasma beta is $\beta = 8\pi n_e k_B T_e / B^2 \approx 5$, hence the B field should negligibly affect the overall plasma dynamics except for the aforementioned thermal transport.

To go beyond the above estimates, we have performed a 3D MHD simulation of the L1 and L2 beam-gas interaction with the FLASH code [37], using the same parameters as in the experiment. This simulation, which accounts for anisotropic (electron and ion) thermal diffusion in the magnetized case, aims to predict the macroscopic plasma density and temperature evolutions. However, for the interpretation of the SRS measurement, we will turn to kinetic PIC simulations. **Details about the MHD simulation setup can be found in the Supplemental Material [38–40].**

The simulated electron density and temperature profiles are shown in Figs. 3(a) and (b) at time $t = 1 \text{ ns}$. As expected, one clearly observes the formation of a hotter, partially electron-evacuated channel in the magnetized plasma [compare Figs. 3(b1) and 3(b2)]. In turn, the higher electron temperature translates into a faster channel expansion perpendicularly to the laser path [compare Figs. 3(a1) and 3(a2)]. These results are consistent with the weaker beam self-focusing inferred from the HISAC measurements. The inhibition of thermal transport across the B field further accounts from the sharper temperature gradient along the laser path.

We now discuss the results of the backscattered light diagnostics. We first note that our SRS diagnostic does not highlight any significant effect of the external B field on SRS. This is ascribed to the fact that, in our conditions ($n_i \simeq 0.02 - 0.08n_c$, $T_e \simeq 100 \text{ eV}$, $I_0 \simeq 10^{15} \text{ W cm}^{-2}$), the backward SRS growth rate, $\Gamma_{\text{SBS}} \simeq \frac{\omega_{pi}}{2\sqrt{2}} \frac{v_{osc}}{c} (\frac{c}{c_s})^{1/2} \simeq 3.6 \times 10^{12} \text{ s}^{-1}$ (ω_{pi} is the ion plasma frequency and c_s the acoustic speed $\propto \sqrt{T_e}$), evaluated in the unmagnetized, weak-coupling limit [11], weakly depends on the electron temperature ($\Gamma_{\text{SBS}} \propto T_e^{-1/4}$) and greatly exceeds the ion

cyclotron frequency $\omega_{ci} \simeq 1.9 \times 10^9 \text{ s}^{-1}$.

By contrast, our measurements reveal an impact of the 20-T B field on backward SRS. Figure 4(a) reports the SRS data obtained under various density conditions. Although the SRS reflectivity remains weak ($\sim 10^{-5}$) in all cases, as expected in our conditions [41], mainly because of the low plasma density, it is clearly enhanced in the presence of the B field. Note that while preliminary studies [18, 25] revealed a mitigating effect of an external B field on SRS, a more recent work [42] has shown either a reduction or an increase in SRS depending on the laser and plasma conditions [42].

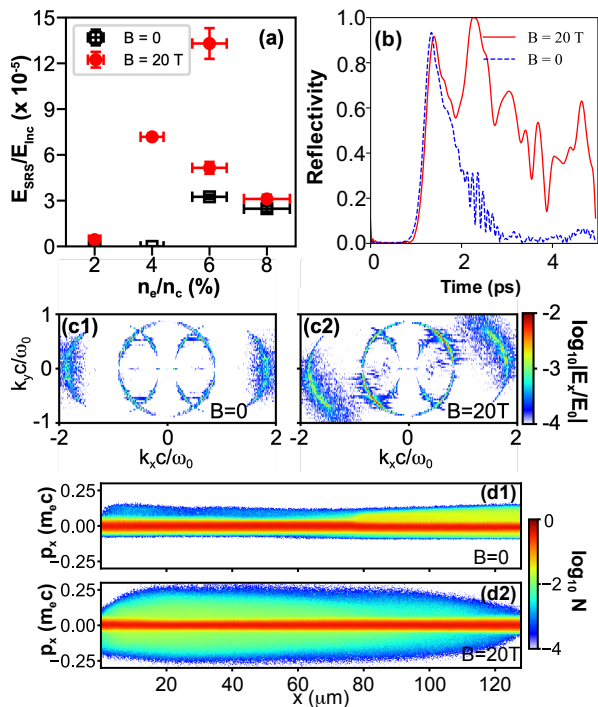


FIG. 4. (a) Experimentally measured backscattered SRS light energy (normalized to the incident laser energy) for various peak electron densities, and with (red dots) or without (black triangles) an external 20 T B field. The horizontal error bars represent the calibration uncertainty, while the vertical error bars represent the noise level of the corresponding shots. (b) Time evolution of the backward SRS reflectivity from 2D PIC simulations with $n_e = 0.02 n_c$, $T_e = 200 \text{ eV}$, $a_0 = 0.033$, $B = 0 \text{ T}$ (blue dashed curve) or $B = 20 \text{ T}$ (red solid curve). The two curves are normalized to the maximum value of the magnetized case, which is reached at around 2.2 ps. Panels (c) and (d) display the (c) 2D FFT of the simulated longitudinal (SRS-driven) E_x field (normalized to the incident laser field) and (d) $x - p_x$ electron phase space in the (c1,d1) unmagnetized and (c2,d2) magnetized regimes, at time $t = 5.2 \text{ ps}$, and in \log_{10} scale.

We have used the SMILEI PIC code [43] to investigate, in 2D geometry, the effect of a 20-T external B field on backward SRS. This field is here directed along the z axis and the laser propagates along x , as in the experi-

ment. Though, unlike in the experiment, the laser field is polarized along y in order for the plasma motion to be confined in the (x, y) simulation plane. The plasma, initialized with a peak electron density $n_e = 0.02 n_c$, and a uniform electron temperature $T_e = 200 \text{ eV}$, is subjected to a plane laser wave of dimensionless amplitude $a_0 = eE_y/m_e c \omega_0 = 0.033$. The simulation setup is further detailed in the Supplemental Material.

Figure 4(b) compares, with or without B field, the time histories of the SRS reflectivity. The SRS activity turns out to wane after $\sim 1.4 \text{ ps}$ in the unmagnetized case, while in the magnetized case it continues afterwards with a bursty evolution. From unmagnetized linear theory, the fastest-growing wavenumber of backward SRS is $k_x \simeq 0.25 \lambda_D^{-1}$ (λ_D is the electron Debye length), implying that the instability operates in the kinetic regime [44]. This is consistent with the spectral peaks seen in both configurations at $k_x c/\omega_0 \simeq \pm 1.8$ in the 2D Fourier transforms of the E_x field [Figs. 4(c1) and (c2)]. Moreover, as the theoretical magnetized SRS growth rate [24] verifies $a_0 \ll 1$ and $\omega_{ce} \ll \omega_{pe}$, the instability should not be directly affected by the B field [see details in Fig. S3(b)], which is well corroborated by the similar evolutions of the SRS reflectivity in Fig. 4(b) before 2 ps. However, Fig. 4(c2) indicates that in the magnetized case, the Langmuir waves are excited over a broader angular range and along significantly oblique directions ($k_y/k_x \sim 0.3$).

The origin of the enhanced SRS lies in the longitudinal magnetic confinement of the suprathermal electrons energized by the SRS-driven, nonlinear Langmuir waves. This is clearly seen by comparing the unmagnetized and magnetized $x - p_x$ electron phase spaces at time $t = 5.2 \text{ ps}$ [Figs. 4(d1) and (d2)]. Without B field, those electrons mainly drift along $x > 0$ whereas in the magnetized case, they are significantly hotter (reaching $v_x \sim 0.25 c$ velocities, i.e., $\sim 15 \text{ keV}$ energies) and, due to magnetic reflection, move in equal numbers along both $x > 0$ and $x < 0$. The latter behavior is consistent with the estimated $\sim 20 \mu\text{m}$ Larmor radius and $\sim 1.8 \text{ ps}$ Larmor period of those electrons. Note that the latter Larmor period precisely corresponds to the time at which the SRS activities between the magnetized and unmagnetized cases start to depart from each other.

In summary, we have investigated, for the first time experimentally, how the presence of an external, $\sim 20 \text{ T}$ B field can modify the propagation and energy coupling of a $10^{15} \text{ W cm}^{-2}$, 1 ns laser pulse in an undercritical ($n_e = 0.02 - 0.08 n_c$) plasma. First, we have found that the (inverse Bremsstrahlung-dominated) laser transmission can be significantly increased (up to twofold at $n_e \simeq 0.04 n_c$) due to the creation of a hotter, more dilute plasma channel, and that the laser propagation itself is improved. This is observed as the transmitted light is less self-focused and more homogeneous – an interesting result for mitigating illumination nonuniformities in

ICF scenarios. Second, we have demonstrated enhanced backward SRS in the magnetized case, which according to kinetic simulations, arises from the magnetic confinement of the SRS-driven suprathermal electrons. The latter effect may also be favorable to ICF in lowering the preheating of the target by these electrons [45]. Finally, our results could also benefit other branches of research, such as SRS-based laser compression [46] and amplification [47, 48] schemes. The next steps will include systematically investigating the effect of the relative orientation of the magnetic field versus the laser propagation axis and polarization, as well as more varied plasma conditions [42].

This work was supported by the European Research Council (ERC) under the European Union’s Horizon 2020 research and innovation program (Grant Agreement No. 787539). The authors acknowledge the expertise of the LULI laser facility staff. The computational resources of this work were supported by the National Sciences and Engineering Research Council of Canada (NSERC) and Compute Canada (Job: pve-323-ac, PA).

* yao.weipeng@polytechnique.edu

† julien.fuchs@polytechnique.edu

- [1] J. Nuckolls, L. Wood, A. Thiessen, and G. Zimmerman, *Laser compression of matter to super-high densities: Thermonuclear (CTR) applications*, *Nature* **239**, 139–142 (1972).
- [2] W. L. Kruer, *Intense laser plasma interactions: From Janus to Nova*, *Physics of Fluids B: Plasma Physics* **3**, 2356–2366 (1991).
- [3] A. Zylstra, O. Hurricane, D. Callahan, A. Kritcher, J. Ralph, H. Robey, J. Ross, C. Young, K. Baker, D. Casey, *et al.*, *Burning plasma achieved in inertial fusion*, *Nature* **601**, 542–548 (2022).
- [4] R. Craxton, K. Anderson, T. Boehly, V. Goncharov, D. Harding, J. Knauer, R. McCrory, P. McKenty, D. Meyerhofer, J. Myatt, *et al.*, *Direct-drive inertial confinement fusion: A review*, *Physics of Plasmas* **22**, 110501 (2015).
- [5] J. Lindl, *Development of the indirect-drive approach to inertial confinement fusion and the target physics basis for ignition and gain*, *Physics of plasmas* **2**, 3933–4024 (1995).
- [6] A. Casner, *Recent progress in quantifying hydrodynamics instabilities and turbulence in inertial confinement fusion and high-energy-density experiments*, *Philosophical Transactions of the Royal Society A* **379**, 20200021 (2021).
- [7] J. Fuchs, C. Labaune, S. Depierreux, H. Baldis, A. Michard, and G. James, *Experimental evidence of plasma-induced incoherence of an intense laser beam propagating in an underdense plasma*, *Physical Review Letters* **86**, 432 (2001).
- [8] V. Malka, J. Faure, S. Hüller, V. Tikhonchuk, S. Weber, and F. Amiranoff, *Enhanced spatiotemporal laser-beam smoothing in gas-jet plasmas*, *Physical review letters* **90**, 075002 (2003).
- [9] D. Pesme, S. Hüller, J. Myatt, C. Riconda, A. Maximov, V. Tikhonchuk, C. Labaune, J. Fuchs, S. Depierreux, and H. Baldis, *Laser-plasma interaction studies in the context of megajoule lasers for inertial fusion*, *Plasma physics and controlled fusion* **44**, B53 (2002).
- [10] L. Lancia, M. Grech, S. Weber, J.-R. Marquès, L. Romaini, M. Nakatsutsumi, P. Antici, A. Bellue, N. Bourgeois, J.-L. Feugeas, *et al.*, *Anomalous self-generated electrostatic fields in nanosecond laser-plasma interaction*, *Physics of Plasmas* **18**, 030705 (2011).
- [11] D. S. Montgomery, *Two decades of progress in understanding and control of laser plasma instabilities in indirect drive inertial fusion*, *Phys. Plasmas* **23**, 055601 (2016).
- [12] W. L. Kruer, *The physics of laser plasma interaction* (Addison-Wesley, New York, 1988).
- [13] P. Chang, G. Fiksel, M. Hohenberger, J. Knauer, R. Betti, F. Marshall, D. Meyerhofer, F. Séguin, and R. Petrasso, *Fusion yield enhancement in magnetized laser-driven implosions*, *Physical review letters* **107**, 035006 (2011).
- [14] D. Montgomery, B. J. Albright, D. Barnak, P. Chang, J. Davies, G. Fiksel, D. Froula, J. Kline, M. MacDonald, A. Sefkow, *et al.*, *Use of external magnetic fields in hohlraum plasmas to improve laser-coupling*, *Physics of Plasmas* **22**, 010703 (2015).
- [15] J. Moody, B. Pollock, H. Sio, D. Strozzi, D.-M. Ho, C. Walsh, G. Kemp, B. Lahmann, S. Kucheyev, B. Koziowski, *et al.*, *Increased Ion Temperature and Neutron Yield Observed in Magnetized Indirectly Driven D 2-Filled Capsule Implosions on the National Ignition Facility*, *Physical Review Letters* **129**, 195002 (2022).
- [16] L. Perkins, D.-M. Ho, B. Logan, G. Zimmerman, M. Rhodes, D. Strozzi, D. Blackfield, and S. Hawkins, *The potential of imposed magnetic fields for enhancing ignition probability and fusion energy yield in indirect-drive inertial confinement fusion*, *Physics of plasmas* **24**, 062708 (2017).
- [17] H. Watkins and R. Kingham, *Magnetised thermal self-focusing and filamentation of long-pulse lasers in plasmas relevant to magnetised ICF experiments*, *Physics of Plasmas* **25**, 092701 (2018).
- [18] T. Gong, J. Zheng, Z. Li, Y. Ding, D. Yang, G. Hu, and B. Zhao, *Mitigating stimulated scattering processes in gas-filled hohlraums via external magnetic fields*, *Physics of Plasmas* **22**, 092706 (2015).
- [19] M. R. Gomez, S. A. Slutz, A. B. Sefkow, D. B. Sinars, K. D. Hahn, S. B. Hansen, E. C. Harding, P. F. Knapp, P. F. Schmit, C. A. Jennings, *et al.*, *Experimental demonstration of fusion-relevant conditions in magnetized liner inertial fusion*, *Physical review letters* **113**, 155003 (2014).
- [20] Y. Shi, *Three-wave interactions in magnetized warm-fluid plasmas: General theory with evaluable coupling coefficient*, *Physical Review E* **99**, 063212 (2019).
- [21] Z. Liu, B. Li, J. Xiang, L. Cao, C. Zheng, and L. Hao, *Faraday effect on stimulated Raman scattering in the linear region*, *Plasma Physics and Controlled Fusion* **60**, 045008 (2018).
- [22] E. Los and D. Strozzi, *Magnetized Laser-Plasma Interactions in High-Energy-Density Systems: Parallel Propagation*, arXiv preprint arXiv:2111.00224 (2021).
- [23] K. Hassoon, H. Salih, and V. Tripathi, *Stimulated Raman*

- forward scattering of a laser in a plasma with transverse magnetic field, *Physica Scripta* **80**, 065501 (2009).
- [24] A. Paknezhad and D. Dorrnian, *Nonlinear backward Raman scattering in the short laser pulse interaction with a cold underdense transversely magnetized plasma*, *Laser and Particle Beams* **29**, 373–380 (2011).
- [25] B. Winjum, F. Tsung, and W. Mori, *Mitigation of stimulated Raman scattering in the kinetic regime by external magnetic fields*, *Physical Review E* **98**, 043208 (2018).
- [26] D. Montgomery, R. Johnson, H. Rose, J. Cobble, and J. Fernández, *Flow-induced beam steering in a single laser hot spot*, *Physical Review Letters* **84**, 678 (2000).
- [27] B. Wattellier, J. Fuchs, J.-P. Zou, J.-C. Chanteloup, H. Bandulet, P. Michel, C. Labaune, S. Depierreux, A. Kudryashov, and A. Aleksandrov, *Generation of a single hot spot by use of a deformable mirror and study of its propagation in an underdense plasma*, *JOSA B* **20**, 1632–1642 (2003).
- [28] P. Masson-Laborde, S. Hüller, D. Pesme, C. Labaune, S. Depierreux, P. Loiseau, and H. Bandulet, *Stimulated Brillouin scattering reduction induced by self-focusing for a single laser speckle interacting with an expanding plasma*, *Physics of Plasmas* **21**, 032703 (2014).
- [29] M. Vandenboomgaerde, J. Bastian, A. Casner, D. Galmiche, J.-P. Jadaud, S. Laffite, S. Liberatorre, G. Malinie, and F. Philippe, *Prolate-Spheroid (“Rugby-Shaped”) Hohlräum for Inertial Confinement Fusion*, *Physical Review Letters* **99**, [10.1103/physrevlett.99.065004](https://doi.org/10.1103/physrevlett.99.065004) (2007).
- [30] D. Froula, J. Ross, B. Pollock, P. Davis, A. James, L. Divol, M. Edwards, A. Offenberger, D. Price, R. Town, *et al.*, *Quenching of the nonlocal electron heat transport by large external magnetic fields in a laser-produced plasma measured with imaging Thomson scattering*, *Physical review letters* **98**, 135001 (2007).
- [31] B. Albertazzi, J. Béard, A. Ciardi, T. Vinci, J. Albrecht, J. Billette, T. Burris-Mog, S. Chen, D. Da Silva, S. Dittrich, *et al.*, *Production of large volume, strongly magnetized laser-produced plasmas by use of pulsed external magnetic fields*, *Review of Scientific Instruments* **84**, 043505 (2013).
- [32] D. Higginson, G. Revet, B. Khair, J. Béard, M. Blecher, M. Borghesi, K. Burdonov, S. Chen, E. Filippov, D. Khaghani, *et al.*, *Detailed characterization of laser-produced astrophysically-relevant jets formed via a poloidal magnetic nozzle*, *High Energy Density Physics* **23**, 48–59 (2017).
- [33] R. Kodama, K. Okada, and Y. Kato, *Development of a two-dimensional space-resolved high speed sampling camera*, *Review of scientific instruments* **70**, 625–628 (1999).
- [34] M. Nakatsutsumi, J. Marques, P. Antici, N. Bourgeois, J. Feugeas, T. Lin, P. Nicolai, L. Romagnani, R. Kodama, P. Audebert, *et al.*, *High-power laser delocalization in plasmas leading to long-range beam merging*, *Nature Physics* **6**, 1010–1016 (2010).
- [35] D. H. Froula, D. Bower, M. Chrisp, S. Grace, J. H. Kamperschroer, T. M. Kelleher, R. K. Kirkwood, B. MacGowan, T. McCarville, N. Sewall, F. Y. Shimamoto, S. J. Shiromizu, B. Young, and S. H. Glenzer, *Full-aperture backscatter measurements on the National Ignition Facility*, *Review of Scientific Instruments* **75**, 4168–4170 (2004).
- [36] A. Richardson, *2019 NRL Plasma Formulary* (Naval Research Laboratory Washington, DC, 2019).
- [37] B. Fryxell, K. Olson, P. Ricker, F. Timmes, M. Zingale, D. Lamb, P. MacNeice, R. Rosner, J. Truran, and H. Tufo, *FLASH: An adaptive mesh hydrodynamics code for modeling astrophysical thermonuclear flashes*, *The Astrophysical Journal Supplement Series* **131**, 273 (2000).
- [38] A. Ciardi, S. Lebedev, A. Frank, E. Blackman, J. Chittenden, C. Jennings, D. Ampleford, S. Bland, S. Bott, J. Rapley, *et al.*, *The evolution of magnetic tower jets in the laboratory*, *Physics of Plasmas* **14**, 056501 (2007).
- [39] D. Gray, J. Kilkenny, M. White, P. Blyth, and D. Hull, *Observation of severe heat-flux limitation and ion-acoustic turbulence in a laser-heated plasma*, *Physical Review Letters* **39**, 1270 (1977).
- [40] E. Chatzopoulos and K. Weide, *Gray Radiation Hydrodynamics with the FLASH Code for Astrophysical Applications*, *The Astrophysical Journal* **876**, 148 (2019).
- [41] T. Gong, L. Hao, Z. Li, D. Yang, S. Li, X. Li, L. Guo, S. Zou, Y. Liu, X. Jiang, X. Peng, T. Xu, X. Liu, Y. Li, C. Zheng, H. Cai, Z. Liu, J. Zheng, Z. Wang, Q. Li, P. Li, R. Zhang, Y. Zhang, F. Wang, D. Wang, F. Wang, S. Liu, J. Yang, S. Jiang, B. Zhang, and Y. Ding, *Recent research progress of laser plasma interactions in Shenguang laser facilities*, *Matter and Radiation at Extremes* **4**, 055202 (2019).
- [42] B. Winjum, R. Lee, S. Bolanos, F. Tsung, W. Mori, *et al.*, in *APS Division of Plasma Physics Meeting Abstracts*, Vol. 2021 (2021) pp. TO04–007.
- [43] J. Derouillat, A. Beck, F. Pérez, T. Vinci, M. Chiramello, A. Grassi, M. Flé, G. Bouchard, I. Plotnikov, N. Aunai, *et al.*, *Smilei: A collaborative, open-source, multi-purpose particle-in-cell code for plasma simulation*, *Computer Physics Communications* **222**, 351–373 (2018).
- [44] J. Kline, D. Montgomery, L. Yin, D. DuBois, B. Albright, B. Bezerides, J. Cobble, E. Dodd, D. DuBois, J. Fernández, *et al.*, *Different $k \lambda d$ regimes for nonlinear effects on Langmuir waves*, *Physics of plasmas* **13**, 055906 (2006).
- [45] A. Solodov, M. Rosenberg, W. Seka, J. Myatt, M. Hohenberger, R. Epstein, C. Stoeckl, R. Short, S. Regan, P. Michel, *et al.*, *Hot-electron generation at direct-drive ignition-relevant plasma conditions at the National Ignition Facility*, *Physics of Plasmas* **27**, 052706 (2020).
- [46] V. Malkin, G. Shvets, and N. Fisch, *Fast compression of laser beams to highly overcritical powers*, *Physical review letters* **82**, 4448 (1999).
- [47] K. Qu, I. Barth, and N. J. Fisch, *Plasma wave seed for Raman amplifiers*, *Physical review letters* **118**, 164801 (2017).
- [48] Y. Shi, H. Qin, and N. J. Fisch, *Laser-plasma interactions in magnetized environment*, *Physics of Plasmas* **25**, 055706 (2018).